Published in final edited form as:
Cell Metab. 2014 September 2; 20(3): 499–511. doi:10.1016/j.cmet.2014.06.008.

A macrophage NBR1-MEKK3 complex triggers JNK-mediated adipose-tissue inflammation in obesity

Eloy D. Hernandez[1,4], **Sang Jun Lee**[1,4], **Ji Young Kim**[1], **Angeles Duran**[1], **Juan F. Linares**[1], **Tomoko Yajima**[1], **Timo D. Müller**[2], **Matthias H. Tschöp**[2], **Steven R. Smith**[3], **Maria T. Diaz-Meco**[1], and **Jorge Moscat**[1,5]

[1]Sanford-Burnham Medical Research Institute, 10901 N. Torrey Pines Road, La Jolla, CA 92037, USA

[2]Institute for Diabetes and Obesity, Helmholtz Diabetes Center, Helmholtz Zentrum München & Division of Metabolic Diseases, Department of Medicine, Technische Universität München, 85764 Munich, Germany

[3]Translational Research Institute for Metabolism and Diabetes, Florida Hospital, Sanford-Burnham Medical Research Institute, FL 32789, USA

SUMMARY

The c-Jun NH(2)-terminal kinase (JNK) is a critical determinant of obesity-associated inflammation and glucose intolerance. The upstream mechanisms controlling this pathway are still unknown. Here we report that the levels of the PB1 domain-containing adapter NBR1 correlated with the expression of pro-inflammatory molecules in adipose tissue from human patients with metabolic syndrome, suggesting that NBR1 plays a key role in adipose-tissue inflammation. We also show that NBR1 inactivation in the myeloid compartment impairs the function, M1 polarization and chemotactic activity of macrophages, prevents inflammation of adipose tissue, and improves glucose tolerance in obese mice. Furthermore, we demonstrate that an interaction between the PB1 domains of NBR1 and the mitogen-activated kinase kinase 3 (MEKK3) enables the formation of a signaling complex required for the activation of JNK. Together these discoveries identify an NBR1-MEKK3 complex as a key regulator of JNK signaling and adipose-tissue inflammation in obesity.

[5]Corresponding author: Jorge Moscat (jmoscat@sanfordburnham.org).
[4]Equal contribution

AUTHOR CONTRIBUTIONS

E.D.H and S.J.L. performed most of experiments of this study with equal contribution. J.Y.K. contributed to GTT and ITT experiments. A.D. and E.D.H. performed immunofluorescence analysis, FACS isolation of ATMs and pull-down experiments. J.F.L. contributed to NBR1 expression analyses and MLK3 activity. T.Y. generated NBR1 mutants and expression plasmids; T.D.M. performed gene-expression analysis. T.D.M. and M. H. T. analyzed metabolic phenotype data. S.R.S. contributed to the human studies. M.T.D-M. and J.M conceived and supervised the project; M.T.D-M. and J.M. wrote the manuscript with assistance from all the authors.

INTRODUCTION

Obesity is an international healthcare priority due to its increasing prevalence and its association with glucose intolerance (Spiegel and Nabel, 2006; Yach et al., 2006). The lack of a complete understanding of the precise regulatory networks that control adipogenesis, energy expenditure, and inflammation is a fundamental problem in metabolic research. It is clear also that obesity-induced inflammation underlies critical aspects of glucose metabolism deregulation and insulin resistance (Glass and Olefsky, 2012; Gregor and Hotamisligil, 2011). We recently identified a signaling molecule that plays important roles in obesity and the inflammation and glucose intolerance that develop in the context of this condition. Specifically, genetic ablation of the signaling adapter p62 (also known as sequestosome 1) in mice resulted in mature-onset obesity, adipose inflammation and glucose intolerance (Rodriguez et al., 2006). Notably, p62 is a member of the PB1 domain-containing signaling network, which also includes kinases such as protein kinase C ζ (PKCζ), mitogen-activated protein kinase kinase 2 (MEKK2) and MEKK3, as well as adapters such as partitioning-defective protein 6 (Par6) and NBR1 (Moscat et al., 2006). It is believed that p62 can interact alternatively with PKCζ or NBR1 through their respective PB1 domains, but the physiological role and mechanisms of action of NBR1 in vivo have not yet been clarified (Moscat and Diaz-Meco, 2011; Moscat et al., 2006; Moscat et al., 2007, 2009). Although PKCζ-deficient mice do not show alterations in adiposity as compared to WT mice when both are fed with high-fat diet (HFD), PKCζ-deficient mice showed increased adipose inflammation and impaired glucose tolerance (Lee et al., 2010).

Our data on p62 knock-out (KO) mice and cells have demonstrated that p62 is a critical negative regulator of white adipose tissue (WAT) adipogenesis but a positive regulator of brown adipose tissue (BAT) function, through the negative regulation of ERK1 and the positive regulation of p38, respectively (Muller et al., 2013). This model explains why the adipose-specific ablation of p62 in mice results not only in an increase in adiposity but also impaired non-shivering thermogenesis, which in turn leads to a decrease in the metabolic rate (Muller et al., 2013). The fact that PKCζ is a negative regulator of obesity-induced inflammation is of great functional relevance, since recent studies have highlighted the importance of inflammation in the induction of glucose intolerance in obese mice (Hotamisligil, 2006; Qatanani and Lazar, 2007; Schenk et al., 2008; Shoelson et al., 2006; Solinas et al., 2007). Also, experiments from a number of research groups have demonstrated that the ablation of macrophages in mice normalizes glucose homeostasis in the context of obesity (Gordon, 2003; Gordon and Taylor, 2005; Lumeng et al., 2007a; Lumeng et al., 2007b; Lumeng et al., 2007c; Mantovani et al., 2004; Patsouris et al., 2008). Interestingly, selective genetic inactivation of p62 in the myeloid compartment using cell-specific Cre mouse lines revealed that p62 does not have an impact on macrophages in the adipose tissue of obese mice (Muller et al., 2013). This finding suggests that the enhanced inflammation in the total body p62-deficient mouse is secondary to increased adiposity and not due to a potential role of p62 in the myeloid compartment.

The domain organization of NBR1 is remarkably similar to that of p62, featuring PB1, zinc-finger, and UBA domains. The outcomes of overexpression and transfection studies have suggested that NBR1 is involved in growth-factor trafficking (Mardakheh et al., 2009)

and/or p62-mediated processes (Kirkin et al., 2009; Lange et al., 2005; Yang et al., 2010). However, its precise in vivo contribution to the control of metabolic homeostasis and/or the ensuing inflammation in the context of obesity has not been investigated. It is possible that p62, PKCζ, and NBR1 play different roles in the control of metabolic homeostasis depending on cell type. Here, we have characterized the effect of myeloid-specific NBR1 ablation, and found that this protein plays a critical role in the regulation of macrophage polarization toward the M1 phenotype during obesity-induced inflammation. Our studies in human patients with metabolic syndrome revealed a significantly positive correlation between NBR1 transcript levels and markers of metabolic alterations and inflammation. These results establish that NBR1 plays a critical role in obesity-induced glucose intolerance, and that this is due to its impact on macrophage function. They also highlight the relevance of the PB1 network comprised of p62, PKCζ and NBR1 at the cellular interface between metabolism and inflammation.

RESULTS

High NBR1 levels correlate with obesity in human patients

The initial evidence of a possible connection between NBR1 and abnormalities in metabolic homeostasis and obesity-induced inflammation came from our analysis of adipose tissues from two cohorts of human patients. The first consisted of sixty-three young and basically healthy men and women with a wide range of body mass index (BMI) and body fat values [see (Ukropcova et al., 2007) for subject characteristics]. We found a positive and significant statistical correlation between NBR1 and PPARγ ($r= 0.36$, $p= 0.003$) transcript levels in this cohort (data not shown), which suggested that NBR1 and PPARγ could act in the same pathway to control metabolic homeostasis in adipose tissue of obese but generally healthy patients. This conclusion was supported by analysis of a second cohort, which consisted of 44 middle-aged men with NCEP-defined “metabolic syndrome” (Grundy et al., 2004) (Table S1). This population is characterized by more adipose tissue inflammation than the healthy population in the study described above, and we found a highly significant positive correlation between NBR1 transcript levels and not only PPARγ1 and PPARγ2, (Figures 1A and 1B) but also markers of the monocyte and macrophage lineage, such as CD68 and CD163 (Figures 1C and 1D). Notably, the latter have been validated as markers of macrophage infiltration based on immunohistochemistry (data not shown). Significant correlations were also found with transcripts encoding chemokines and pro-inflammatory proteins like MCP-1 and MIP-1 (Figures 1E and 1F). These results suggest a potential role of NBR1 in obesity-induced inflammation.

NBR1 in the myeloid compartment plays a critical role in obesity-induced inflammation

Intrigued by the potential of a macrophage-based link between NBR1, adipose-tissue inflammation and metabolic syndrome, we next investigated the expression of NBR1 in the adipose-tissue of obese WT mice fed a high-fat diet (HFD) as compared to lean mice fed a regular chow diet (RD). Double immunofluorescence of NBR1 and the macrophage marker, F4/80 showed NBR1 staining exclusively in crown-like structures that colocalized with F4/80 mostly in the HFD adipose sections, which indicates that NBR1 is specifically expressed in macrophages that infiltrate obese adipose tissue (Figure 2A). Consistent with

this, NBR1 mRNA levels were significantly increased in adipose tissue macrophages (ATMs) isolated from obese as compared to lean mice (Figure 2B). Therefore, to address the role of NBR1 in adipose-tissue inflammation in vivo, we generated mice in which NBR1 was genetically and selectively inactivated in the myeloid cell compartment. Specifically $NBR1^{fl/fl}$ mice were crossed to lysozyme M (LysM) cre mice. This mouse line (herein termed $NBR1^{My}KO$) and their corresponding $NBR1^{fl/fl}$ wild-type (WT) controls were fed a high-fat diet (HFD) for 12 weeks, and body weight was monitored continuously. The results in Figure 2C confirm that NBR1 was effectively and selectively deleted from macrophages. The lack of NBR1 in the myeloid compartment did not affect the body weight or fat content of these mice, regardless of whether they were fed the HFD (Figures 2D and 2E) or regular chow diet, and even when monitored over a longer period (not shown). However, in the mutant mice, macrophage recruitment to the adipose tissue was significantly impaired (Figure 2F), and the levels of inflammatory markers in the white adipose tissue (WAT) were also reduced (Figure 2G). FACS analysis confirms a reduced presence of ATMs in the WAT of mutant mice (Figures 2H and S1A). It has been established that ATMs can differentiate along different lineages, including the so-called M1 and M2 (Gordon, 2003; Kang et al., 2008; Odegaard et al., 2008; Vats et al., 2006), and an increase in the M1/M2 ratio has been proposed to be responsible for glucose intolerance responses in obese mice (Kang et al., 2008; Odegaard et al., 2008). When isolated ATMs from WT and $NBR1^{My}KO$ mice were analyzed for several markers of macrophage differentiation, it was clear that the loss of NBR1 selectively impaired M1 polarization with a slight although reproducible increase in M2 polarization (Figure 2I). Macrophage infiltration was also inhibited in the livers from $NBR1^{My}KO$ mice as compared to identically treated WT controls, as determined by the levels of macrophage transcript markers CD68 and F4/80 (Figure S1B). Results of Figure S1C show that livers from KO mice displayed a reduction in the expression of genes associated with M1 polarization (TNFα, IL-6, and MCP-1) and an increase in the expression of the M2 polarization marker Mgl2. Of note, although not reaching stastical significance, the circulating levels of TNFα and IL-6 were decreased in KO mice (Figure S1D). Furthermore, the levels of circulating MCP1 were significantly decreased in the serum of KO mice (Figure S1E), consistent with previously published studies demonstrating the role of this chemokine in the recruitment of inflammatory macrophages to obese adipose tissue (Takahashi et al., 2003).

NBR1 deficiency in macrophages improves glucose metabolism

In order to address whether the defects in macrophage polarization of mutant mice affects glucose homeostasis, HFD-fed $NBR1^{My}KO$ mice where compared to identically treated WT controls in terms of glucose tolerance and insulin response. As demonstrated in Figure 3A, NBR1 deficiency in macrophages resulted in improved glucose clearance in glucose tolerance tests. Likewise, NBR1 deficiency in macrophages resulted in improved insulin responses in insulin tolerance tests (Figure 3B), and activation of Akt in liver, muscle and WAT (Figure 3C). In contrast, no differences were found in glucose tolerance and insulin response assays between both mouse genotypes when fed regular chow diet (Figures S2A and S2B). These findings suggest that a lack of NBR1 in the myeloid compartment improves glucose metabolism in the context of chronic HFD exposure. Consistent with this, fasting basal glucose (Figure 3D) and insulin (Figure 3E) levels were significantly reduced in the

mutant mice, as were the transcript levels of liver PEPCK and G6Pase (Figure 3F). However, and in agreement with the fact that the NBR1^{My}KO mice did not differ from their WT counterparts with respect to body weight and adiposity, the metabolic changes in the context of a HFD diet were not significantly different from those observed in identically treated WT mice (Figures S2C-S2H). A wide range of metabolic parameters was tested, including the whole-body respiratory exchange ratio (RER), diurnal patterns of food and water intake, locomotor activity, and calorie expenditure. Therefore, although the loss of NBR1 in the myeloid compartment had a significant impact on adipose-tissue inflammation and glucose homeostasis, it did not affect fat content or energy utilization at the organismal level.

NBR1 is critical for M1 differentiation and macrophage activation *ex vivo*

In order to gain a more in-depth understanding of the mechanisms whereby NBR1 regulates macrophage function in obesity, we used an *ex vivo* system, whereby bone marrow-derived macrophages (BMDMs) were differentiated along the M1 or M2 lineage. Adipocytes secrete type 2 cytokines, such as IL-13 and IL-4, that skew ATMs towards the anti-inflammatory M2 profile. In contrast to their M1 counterparts, which have a pro-inflammatory profile, M2 ATMs counteract inflammation in vivo. ATMs are induced to differentiate along the M1 lineage when exposed to IFNγ (Gordon, 2003; Kang et al., 2008; Odegaard et al., 2008; Vats et al., 2006). Therefore, BMDMs of both genotypes were incubated with IFNγ or IL-13 to promote M1 or M2 differentiation, respectively. Afterwards, the expression of specific markers of each lineage was determined by qRT-PCR. Notably, BMDMs from NBR1^{My}KO mice had a dramatically reduced ability to respond to IFNγ, as evident from the low levels of induced *IL-6*, *TNFα* and *NOS* transcription, but were sensitive to IL-13, as demonstrated by high levels of *Arg1* and *Mgl2* transcription (Figures 4A and 4B). These results are consistent with NBR1 being required for the differentiation of macrophages along the M1, but not the M2, lineage, and therefore being an important transducer of pro-inflammatory signals. Consistent with this notion, the ability of BMDMs to induce IL-6 production, as measured at either the protein (Figure 4C) or mRNA (Figure 4D) level, in response to endotoxin exposure (lipopolysaccharide, LPS) was also severely blunted in NBR1-deficient macrophages. In order to confirm these observations and rule out hypothetical developmental defects in KO macrophages, macrophage-derived Raw cells were treated with either a shRNA that effectively knocked down NBR1 levels (shNBR1, Figure 4E, inset) or a control shRNA (shNT). Depletion of NBR1 in Raw cells resulted in impaired production of IL-6 in response to LPS stimulation (Figure 4E), reinforcing the hypothesis that NBR1 plays a critical role in the inflammatory activation of macrophages. Because the loss of NBR1 in the myeloid compartment reduced not only WAT inflammation but also the number of macrophages in that tissue (Figures 2F–2I), we next tested if the chemotactic response of the mutant macrophages was affected. To this end, we performed migration assays using a Boyden chamber, and applying the chemoattractant MCP-1. Both Raw cells depleted of NBR1 (Figure 4F) and NBR1^{My}KO BMDMs (Figure 4G) exhibited severely reduced chemotactic activity. Similar results were obtained with undifferentiated monocytes (Figure S3). Collectively, these results demonstrate that NBR1 is a positive regulator of the cell autonomous, pro-inflammatory functions of macrophages.

NBR1 regulates the MEKK2/3-MKK4-JNK pathway in macrophages

To begin to address the signaling pathway whereby NBR1 governs macrophage functions, BMDMs were stimulated with LPS for various periods ranging up to 1 hr, and a number of signaling parameters were evaluated. Whereas JNK activation was reproducibly inhibited in the NBR1^{My}KO BMDMs (Figure 5A), neither the activation of ERK (pERK) nor the phosphorylation and degradation of IκB were affected (Figure 5A). NBR1 knockdown in the macrophage-derived Raw cell line led to a similar suppression of the JNK response to LPS treatment (Figure 5B). JNK is the main MAPK activated upon inflammatory stress and it has been associated with glucose intolerance in HFD-treated mice (Hirosumi et al., 2002). JNK is also required for the polarization of BMDMs to the pro-inflammatory M1 phenotype. Moreover, its deletion in macrophages reduces ATM infiltration as well as inflammation, and enhances the efficiency of glucose metabolism in the context of obesity (Han et al., 2013; Sabio et al., 2008; Vallerie et al., 2008). Therefore, our results demonstrating that NBR1 deficiency resulted in impaired JNK activation in macrophages and that it improved glucose tolerance of mice with a myeloid-specific KO, establishes NBR1 as a key regulator of JNK function in the context of obesity-induced inflammation.

In the next series of experiments we investigated the mechanisms whereby NBR1 regulates JNK activation. Interestingly, whereas activation of the JNK upstream kinase MKK4 was severely suppressed in NBR1^{My}KO BMDMs, that of MKK3/6 was not affected (Figure 5C). When macrophages were stimulated with palmitate, a saturated fatty acid abundant during obesity, we found a robust activation of JNK in the WT cultures but not in NBR1^{My}KO macrophages (Figure 5D). Notably, the synthesis of IL-6 and TNFα was likewise induced by palmitate treatment in WT but not in mutant macrophages (Figure 5E). MKK7 was not activated in either the KO or in WT macrophages (not shown). These results strongly suggest that NBR1 positively regulates JNK through a direct or indirect interaction with MKK4 and/or any its upstream activators (MAPKKKs).

PB1-mediated scaffold role of NBR1 in macrophages

As NBR1 contains a PB1 domain, we reasoned that its most likely immediate target would be a PB1-containing MAPKKK, MEKK2 or MEKK3. We further hypothesized that such an interaction might involve direct contact between an acidic residue in the NBR1 PB1 domain and a basic residue in the N-terminal region of the MEKK2 or MEKK3 PB1 domain (Figure 6A) (Moscat et al., 2006; Nakamura et al., 2010). Interestingly, MEKK3 (Figure 6B), similarly to NBR1 (Figure 2B), was upregulated in ATMs isolated from HFD-fed mice as compared to those from mice fed a regular chow diet. To test this possibility, we ectopically expressed HA-tagged MEKK2 or MEKK3 with Flag-tagged NBR1 in human HEK-293T cells, and then assessed interactions between NBR1 and these kinases by immunoprecipitation followed by immunoblotting. The results in Figure 6C show that, whereas Flag-tagged NBR1 was efficiently immunoprecipitated with HA-tagged MEKK3, this was not the case for HA-tagged MEKK2, establishing that NBR1 interacts specifically with MEKK3. Notably, a D50R mutation in the PB1 domain of NBR1 completely abolished this interaction (Figure 6D). Figure 6E demonstrates that endogenous NBR1 and MEKK3 likewise interact physically.

In vitro studies using recombinant MKK4 protein demonstrate that it was not able to interact with purified NBR1 in a pull-down assay but that the addition of recombinant MEKK3 allowed the co-precipitation of MKK4 and NBR1 (Figure S4A). Consistent with the requirement of the PB1 for MEKK3 interaction with NBR1, the NBR1-D50R mutant completely abolished the in vitro co-precipitation of NBR1 with MKK4 (Figure S4A). In agreement with these in vitro results, pull-down of ectopically expressed GST-MKK4 resulted in co-immunoprecipitation of ectopically expressed NBR1 and MEKK3 (Figure 6F). This demonstrates that MEKK3 acts as a bridge to bring MKK4 and NBR1 together. To test the existence of this complex in an endogenous setting, we next stimulated HEK-293 cells stably expressing hTLR4, MD2 and CD14 with LPS, and then immunoprecipitated endogenous NBR1. Western blotting revealed that the interaction between NBR1 and MEKK3 was not inducible, but that the interaction with MKK4 was (Figure 6G). Notably, treatment of BMDM with palmitate resulted in enhanced expression of NBR1 and MEKK3 (Figure 6H), in accordance with the data of Figure 2B and 6B in ATMs from obese mice. More importantly, under these conditions we also found a clear endogenous NBR1-MEKK3 interaction (Figure 6H). Thus, NBR1 appears to function as an organizer of a MEKK3/MKK4 cassette that is required to activate JNK and an obesity-induced inflammatory response. The fact that the simple overexpression of NBR1 is sufficient to elevate JNK activation to levels comparable to those observed following stimulation with LPS (Figure 6I), further supports the notion that the ability of NBR1 to nucleate a signaling complex is essential for the activation of JNK. In agreement with our hypothesis, the knockdown of MEKK3 in BMDM led to reduced JNK activation, as well as of IL-6 and TNFα synthesis, in response to palmitate stimulation (Figures 6J and 6K). MLK3, another MAP3K like MEKK3, has been shown be activated by saturated free fatty acids and required for JNK activation in embryo fibroblasts, as well as in the adipose tissue of HFD-fed mice (Holzer et al., 2011; Jaeschke and Davis, 2007). However, MLK3 deficiency does not affect obesity or glucose homeostasis in HFD-fed mice (Jaeschke and Davis, 2007). Our data demonstrate that although MLK3 is activated in palmitate-treated macrophages, this is independent of NBR1 (Figure S4B). Consistent with a functional role for the PB1 domains in the interaction between NBR1 and MEKK3, the overexpression of NBR1 but not of a PB1 mutant (D50R) activates JNK in cotransfection with MEKK3 (Figure 6L). Interestingly, similar results were obtained in palmitate-activated cells (Figure 6M). Furthermore, the re-expression of NBR1 WT but not of NBR1-D50R reconstituted JNK activation in response to palmitate in NBR1-deficient BMDMs (Figure 6N).

DISCUSSION

Many studies have demonstrated that obesity-induced inflammation plays a critical role in the generation of the metabolic syndrome, including a dysfunctional glucose metabolism and insulin resistance (Glass and Olefsky, 2012; Gregor and Hotamisligil, 2011). However, the precise signaling cascades accounting for these effects still need to be identified, which is of great importance for the design of more efficacious treatments of type-2 diabetes. In this regard, JNK was recently recognized as an important factor in obesity-induced inflammation, a condition that contributes significantly to aberrant glucose metabolism in obesity (Han et al., 2013; Lanuza-Masdeu et al., 2013; Sabio et al., 2008; Vallerie et al.,

2008; Zhang et al., 2011). The initial observations were that JNK activity was abnormally elevated in obese mice, and that whole-body ablation of JNK1 resulted in decreases in body weight and adiposity in the context of a HFD diet (Hirosumi et al., 2002; Tuncman et al., 2006). Although of great relevance, those results did not distinguish between a role for JNK activity in controlling the inflammation induced by obesity from those effects specific to the control of adiposity itself and obesity. Later studies, in which JNK1 was genetically and selectively inactivated in adipocytes, established that this JNK isoform plays a critical role in the inflammatory phenotype of adipocytes, and only a minor role in that of macrophages, in the context of obesity-induced glucose intolerance (Sabio et al., 2008). However, the most recent data from the same investigators demonstrated that simultaneous genetic inactivation of both JNK1 and JNK2 in the myeloid compartment improved glucose tolerance in these mice, although it did not affect the body weight or adiposity (Han et al., 2013). Other potential mechanisms of action might include the implication of NBR1 in the control of inflammation in β-cells function. However, the fact that insulin actions in ITT and phospho-Akt induction are enhanced in response to insulin injection suggests that the most likely main mechanism of action of macrophage NBR1 is not by controlling insulin secretion. Collectively these data demonstrated that JNK activation in macrophages is a critical step in obesity-induced inflammation and glucose intolerance. However, the upstream activators of this JNK activity in macrophages remained unknown. Our data in the present paper demonstrate that the loss of NBR1 in specifically macrophages largely prevents obesity-induced inflammation in vivo. Moreover, our ex vivo and in vitro results link the PB1 domain-mediated interaction between NBR1 and MEKK3 to JNK activation and the M1 polarization of macrophages.

These observations have to be put in the context of the other PB1 domain proteins, p62 and PKCζ, which have been also implicated in the regulation of obesity and the metabolic alterations associated to this physiopathological condition (Moscat et al., 2006) (Moscat et al., 2007) (Moscat et al., 2009). In this regard, it is quite striking that whereas p62 deficiency results in obesity and that the inflammation associated to the lack of p62 is secondary to increased adiposity, the PKCζ loss selectively promotes inflammation in obese mice without effects on adiposity (Muller et al., 2013; Rodriguez et al., 2006). Interestingly, PKCζ anti-inflammatory actions are mostly confined to the adipocyte, with no effects on the hematopoietic system (Lee et al., 2010). In contrast, NBR1 is a pro-inflammatory signaling adapter in macrophages by nucleating a MEKK3-driven JNK cascade, not only in response to inflammatory signals such as LPS, but more importantly in response to saturated fatty acids like palmitate. The mechanisms whereby palmitate promotes the accumulation of NBR1, and MEKK3, are not known but will be very interesting to address in future studies. Overall, these findings reveal a potentially pharmacologically targetable mechanism underlying JNK activation, and suggest that blocking NBR1 binding to MEKK3 may represent an opportunity to prevent type 2 diabetes in human obesity.

EXPERIMENTAL PROCEDURES

Antibodies and Reagents

Murine IFNγ, IL-13 and MCP-1 were obtained from Peprotech, Inc. Lipopolysaccharide from *Escherichia coli* 0111:B4 was from Sigma-Aldrich. Glutathione sepharose 4b, protein G sepharose 4 fast flow and protein A sepharose 4 fast flow were from GE Healthcare Life Sciences. HisPur Cobalt resin was from Thermo Scientific. EZview red anti-HA affinity gel was from Sigma-Aldrich. Antibodies against HA (sc-805), myc (sc-40), NBR1 (sc-130380), MEKK2 (sc-1088), MEKK4 (sc-166196), MKK4 (sc-837), MKK3/6 (sc-13069), ERK1 (sc-94), p38 (sc-728), TAK1 (sc-7162) and AKT (sc-5298) were from Santa Cruz Biotechnology. Antibodies against pMKK3/6 (#9231S), pMKK4 (#9151S), pMKK7 (#4171S), pJNK (#4668S), pERK (#4370S, pp38 (#9215S), IkBalpha (#4814S), pIkBalpha (#9246S) and pAKT-S473 (#4058S) were from Cell Signaling Technology. Flag (F3165) and β-actin (clone AC-74) antibodies were from Sigma-Aldrich. Antibody against MEKK3 (m79820) was purchased from BD Biosciences. p62 antibody (GP62-C) was from PROGEN Biotechnik GmbH. Antibody against JNK (#551196) was purchased from PharMingen. pCMV5-Flag-NBR1 and pWZL-Flag-NBR1 plasmids were obtained by subcloning mouse NBR1 (NM_008676) into the pCMV5-Flag and pWZL-Flag vectors, respectively. The point mutation resulting in an aspartic acid to arginine substitution at position 50 (D50R) of the NBR1 PB1 domain was engineered into the pCMV5-Flag-NBR1 and pWZL-Flag-NBR1 constructs using the QuikChange site-directed mutagenesis kit (Stratagene) and NBR1D50 primers (Table S2). pEBG-MKK4 (GST-MKK4) plasmid was from Addgene (Plasmid: 21563). pCMV-HA-MEKK2 and pCMV-HA-MEKK3 plasmids were a kind gift from Dr. Frank S. Lee (University of Pennsylvania School of Medicine). MLK3 activity reagents were a kind gift from Dr. Ajay Rana (Loyola University Chicago Stritch School of Medicine).

Mice

$NBR1^{fl/fl}$ mice were described previously (Yang et al., 2010). $NBR1^{fl/fl}$ mice were bred to LysM-cre mice to generate myeloid-specific NBR1-KO ($NBR1^{My}KO$). All genotyping was done by PCR. Animals were maintained under controlled temperature (22.5 °C) and illumination (12 hr dark/light cycle). Mice had free access to water and were fed either standard chow or high fat diets (45%-HFD; D12451 or 60%-HFD, D12492; Research Diets Inc.) ad libitum. To assess glucose tolerance and insulin sensitivity 8-week-old mice were fed a standard chow or a 60% high fat diet for 4 weeks. Mice were injected intraperitoneally with 2 g glucose/kg body weight after overnight fasting (25% D-glucose [Fisher Scientific] in 0.9% saline) for GTT assay. For ITT, mice were injected with 0.5–0.75 U insulin/kg body weight (100 U/ml Novolin R [Novo Nordisk]) after 6 hr fasting. Tail-blood glucose levels were measured by using an ACCU-CHEK Aviva (Roche) glucometer. Insulin concentration was measured in plasma with a kit purchased from Crystal Chem. Measurements of energy expenditure were performed using the indirect calorimetry Oxymax system of the Comprehensive Lab Animal Monitoring System (CLAMS; Columbus Instruments) at UCSD Animal Care Program in mice fed a 45% HFD for 12 weeks. After adaptation for 24 hr, recordings were collected for 72 hr. The Institutional Animal Care and Utilization

Committee approved all procedures, in accordance with the NIH guide for the care and use of laboratory animals.

Human studies

The clinical studies were reviewed and approved by the Pennington Biomedical Research Center Institutional Review Board and all subjects provided written confirmation of informed consent.

Stromal vascular cell isolation

Epididymal adipose tissue was excised and minced in 10 ml of HBSS solution containing 0.5% BSA-Fatty acid free (BSA-FAF). Collagenase II (Sigma C6885, 0.5 mg/ml) was added and the tissue was incubated at 37 °C with shaking (30 min). 10 mM EDTA was added 5 min before the end of the incubation. Larger particles were removed using a 250 μm nylon sieves and the filtrates were centrifuged at 500 *g* for 5 min to separate floating adipocytes. The pelleted SVCs were suspended in erythrocyte lysis buffer (155 mM NH_4Cl, 10 mM $KHCO_3$, 0.1 mM EDTA) and incubated at room temperature for 5 min. The erythrocyte-depleted SVCs were centrifuged at 500 *g* for 5 min, and the pellet was suspended in FACS buffer (PBS containing 25 mM HEPES, 2 mM EDTA and 0.5% FBS). Enrichment of $F4/80^+$ cells was performed by magnetic immunoaffinity with F4/80-APC antibody (BM8, eBioscience) and APC positive selection kit (StemCell Technologies).

Analysis of tissue sections

Histology was performed on WAT following fixation in 10% formalin for 24 hr, dehydration, and embedding in paraffin. Sections (5 μm) were cut and stained using hematoxylin and eosin (H&E). For immunohistochemical detection of F4/80, sections were deparaffinized, rehydrated and treated for antigen retrieval. The Vector Mouse on Mouse (M.O.M.) immunodetection kit was then used according to the manufacturer's protocol (Vector Laboratories). After blocking of endogenous peroxidase activity, the sections were incubated in avidin/biotin blocking solution and M.O.M. mouse Ig-blocking reagent, and then with mouse monoclonal F4/80 antibody (#17-4801, eBioscience) for 30 min. The binding of primary antibody was detected using M.O.M. biotinylated anti-mouse IgG, and visualized using diaminobenzidine as the chromogen. For immunofluorescence, sections were deparafinized as described above and incubated with anti- NBR1 antibody (Thermo Scientific) 1:100 and anti-F4/80 (eBioscience) 1:50, overnight at 4°C. Secondary antibodies were then applied (Alexa fluor 568, A11011; Alexa fluor 488, A11006) 1:500 (Invitrogen). Stained sections were examined under an inverted laser scan microscope (LSM 710 NLO, Zeiss, Germany)

Cell Culture

Raw and HEK-293T cells were from ATCC. HEK-293 hTLR4A/MD2/CD14 cells were from InvivoGen (San Diego, CA). Cells were cultured in DMEM supplemented with 10% FCS, 2 mM L-glutamine, 100 U/ml penicillin and 100 μg/ml streptomycin. In the case of the hTLR4A/MD2/CD14 HEK-293 cells, 10 μg/ml blasticidin and 50 μg/ml hygromycin b were

added to growth medium as recommended by the manufacturer. The detailed cell culture procedures are described in the Supplemental Experimental Procedures.

Bone marrow macrophages

Bone marrow-derived macrophages (BMDMs) were prepared by crushing mouse leg bones in DMEM supplemented with 20% FBS, 100 U/ml penicillin, 100 μg/ml streptomycin, and 2 mM L-glutamine. After being filtered through a 70 μm nylon mesh, cells were plated in 10 cm dishes and incubated for 24 hr. Supernatants containing bone marrow precursors were collected, centrifuged at 1,500 rpm and cultured in differentiation media (DMEM supplemented with 30% L929 supernatant, 15% fetal bovine serum, 5% horse serum, 100 U/ml penicillin, 100 μg/ml streptomycin, 2 mM L-glutamine, 0.1 mM non-essential amino acids, 1 mM sodium pyruvate and 0.5 mM β-mercaptoethanol). Polarization studies were performed using BMDMs (8 days in culture) incubated with 100 ng/ml LPS, 0.8 mM Palmitate, 100 ng/ml IFNγ (M1) or 10 ng/ml IL-13 (M2) for the indicated times.

Retroviral transduction of murine bone marrow

After 2 days of differentiation adherent and non-adherent BM cells were suspended in virus supernatants containing 5 μg/ml polybrene, and seeded in six-well plates (2×10^6 cells per well). Plates were centrifuged 1 hr at 1000 g and incubated at 37 °C and 5% CO2. After 24 hr the transduction was repeated as before, suspending non-adherent cells in new virus supernatants that were combined with the other adherent cells. After 24 hr virus supernatants were replaced with differentiation media and selection antibiotics. Cells were replated after 4 days for the final experiment.

Cytokine secretion

BMDMs or shNBR1 Raw cells were seeded into 6 well plates at 3×10^6 cells/well. The next day, the cells were incubated for 1 hr with serum-free DMEM, followed by 3 hr (BMDMs) or 8 hr (shNBR1 Raw cells) with or without 100 ng/ml LPS. Supernatants were collected, filtered through a 0.45 μm mesh and subjected to IL-6 measurement using BD OptEIA™ Mouse IL-6 ELISA Kit (BD Biosciences). Plasma levels of cytokines (MCP-1, TNFα, IL-6) were subjected to measurement using BD OptEIA™ Mouse IL-6 ELISA Kit and Mouse TNFα ELISA kit (BD Biosciences), and eBioscience Mouse MCP-1 ELISA Ready-SET-Go! ™.

RNA analysis

Total RNA from mouse tissues and cultured cells was isolated using the TRI reagent (Molecular Research Center) and the RNeasy Mini Kit (Qiagen), followed by DNAse treatment. After quantification using a Nanodrop 1000 spectrophotometer (Thermo Scientific), 1 μg of RNA was reverse-transcribed using random primers and MultiScribe Reverse Transcriptase (Applied Biosystems). Gene expression was analyzed by amplifying 50 ng of the complementary DNA, using the CFX96 Real Time PCR Detection System with SYBR Green Master Mix (BioRad) and primers described in Table S2. The amplification parameters were set at 95 °C for 30 s, 58 °C for 30 s and 72 °C for 30 s (40 cycles total). Gene expression values for each sample were normalized to the 18S RNA.

Statistical analyses

Data are presented as the mean ± SEM. Differences between groups were examined for statistical significance using non-parametric Mann-Whitney test. The level of statistical significance was set at $p < 0.05$. All error bars represent SEM.

Supplementary Material

Refer to Web version on PubMed Central for supplementary material.

Acknowledgments

Supported by NIH Grants R01DK088107 (J.M.), R01CA172025 (J.M.), R01CA134530 (M.T.D.-M.), 5P30CA030199 (M.T.D-M. and J.M.), and CCSPG Pilot Project Grant under award 5P30CA030199 (to M.T.D.-M. and S.S.) funded this work. The “healthy population” clinical protocol was supported by U.S. Department of Agriculture Grant 2003-34323-14010 and the National Institutes of Health Clinical Nutrition Research Unit DK072476-01 and GlaxoSmithKline supported the parent “metabolic syndrome” clinical study which was the source of the adipose tissue for this study. We thank Christine Blaumueller for editing this manuscript, Diantha LaVine for the artwork, Xiayu Huang (Bioinformatics core) for statistical analysis, and the personnel of the Cell Imaging, Viral Vectors, Functional Genomics, Animal Facility and Histopathology Shared Resources at SBMRI and the UCSD Animal Care Program for technical assistance. We also thank Hui Xie, PhD, TRI-MD, Florida Hospital, for data and statistical support and Meghan Gabriel, SBMRI, for the human adipose tissue gene expression studies.

References

Glass CK, Olefsky JM. Inflammation and lipid signaling in the etiology of insulin resistance. Cell Metab. 2012; 15:635–645. [PubMed: 22560216]

Gordon S. Alternative activation of macrophages. Nat Rev Immunol. 2003; 3:23–35. [PubMed: 12511873]

Gordon S, Taylor PR. Monocyte and macrophage heterogeneity. Nat Rev Immunol. 2005; 5:953–964. [PubMed: 16322748]

Gregor MF, Hotamisligil GS. Inflammatory mechanisms in obesity. Annu Rev Immunol. 2011; 29:415–445. [PubMed: 21219177]

Grundy SM, Brewer HB Jr, Cleeman JI, Smith SC Jr, Lenfant C. American Heart A National Heart L Blood I. Definition of metabolic syndrome: Report of the National Heart, Lung, and Blood Institute/ American Heart Association conference on scientific issues related to definition. Circulation. 2004; 109:433–438. [PubMed: 14744958]

Han MS, Jung DY, Morel C, Lakhani SA, Kim JK, Flavell RA, Davis RJ. JNK expression by macrophages promotes obesity-induced insulin resistance and inflammation. Science. 2013; 339:218–222. [PubMed: 23223452]

Hirosumi J, Tuncman G, Chang L, Gorgun CZ, Uysal KT, Maeda K, Karin M, Hotamisligil GS. A central role for JNK in obesity and insulin resistance. Nature. 2002; 420:333–336. [PubMed: 12447443]

Holzer RG, Park EJ, Li N, Tran H, Chen M, Choi C, Solinas G, Karin M. Saturated fatty acids induce c-Src clustering within membrane subdomains, leading to JNK activation. Cell. 2011; 147:173–184. [PubMed: 21962514]

Hotamisligil GS. Inflammation and metabolic disorders. Nature. 2006; 444:860–867. [PubMed: 17167474]

Jaeschke A, Davis RJ. Metabolic stress signaling mediated by mixed-lineage kinases. Mol Cell. 2007; 27:498–508. [PubMed: 17679097]

Kang K, Reilly SM, Karabacak V, Gangl MR, Fitzgerald K, Hatano B, Lee CH. Adipocyte-derived Th2 cytokines and myeloid PPARdelta regulate macrophage polarization and insulin sensitivity. Cell Metab. 2008; 7:485–495. [PubMed: 18522830]

Kirkin V, Lamark T, Sou YS, Bjorkoy G, Nunn JL, Bruun JA, Shvets E, McEwan DG, Clausen TH, Wild P, et al. A role for NBR1 in autophagosomal degradation of ubiquitinated substrates. Mol Cell. 2009; 33:505–516. [PubMed: 19250911]

Lange S, Xiang F, Yakovenko A, Vihola A, Hackman P, Rostkova E, Kristensen J, Brandmeier B, Franzen G, Hedberg B, et al. The Kinase Domain of Titin Controls Muscle Gene Expression and Protein Turnover. Science %R 101126/science1110463. 2005; 308:1599–1603.

Lanuza-Masdeu J, Arevalo MI, Vila C, Barbera A, Gomis R, Caelles C. In vivo JNK activation in pancreatic beta-cells leads to glucose intolerance caused by insulin resistance in pancreas. Diabetes. 2013; 62:2308–2317. [PubMed: 23349497]

Lee SJ, Kim JY, Nogueiras R, Linares JF, Perez-Tilve D, Jung DY, Ko HJ, Hofmann SM, Drew A, Leitges M, et al. PKCzeta-regulated inflammation in the nonhematopoietic compartment is critical for obesity-induced glucose intolerance. Cell Metab. 2010; 12:65–77. [PubMed: 20620996]

Lumeng CN, Bodzin JL, Saltiel AR. Obesity induces a phenotypic switch in adipose tissue macrophage polarization. The Journal of clinical investigation. 2007a; 117:175–184. [PubMed: 17200717]

Lumeng CN, Deyoung SM, Bodzin JL, Saltiel AR. Increased inflammatory properties of adipose tissue macrophages recruited during diet-induced obesity. Diabetes. 2007b; 56:16–23. [PubMed: 17192460]

Lumeng CN, Deyoung SM, Saltiel AR. Macrophages block insulin action in adipocytes by altering expression of signaling and glucose transport proteins. American journal of physiology Endocrinology and metabolism. 2007c; 292:E166–174. [PubMed: 16926380]

Mantovani A, Sica A, Sozzani S, Allavena P, Vecchi A, Locati M. The chemokine system in diverse forms of macrophage activation and polarization. Trends Immunol. 2004; 25:677–686. [PubMed: 15530839]

Mardakheh FK, Yekezare M, Machesky LM, Heath JK. Spred2 interaction with the late endosomal protein NBR1 down-regulates fibroblast growth factor receptor signaling. The Journal of cell biology. 2009; 187:265–277. [PubMed: 19822672]

Moscat J, Diaz-Meco MT. Feedback on fat: p62-mTORC1-autophagy connections. Cell. 2011; 147:724–727. [PubMed: 22078874]

Moscat J, Diaz-Meco MT, Albert A, Campuzano S. Cell Signaling and Function Organized by PB1 Domain Interactions. Mol Cell. 2006; 23:631–640. [PubMed: 16949360]

Moscat J, Diaz-Meco MT, Wooten MW. Signal integration and diversification through the p62 scaffold protein. Trends Biochem Sci. 2007; 32:95–100. [PubMed: 17174552]

Moscat J, Diaz-Meco MT, Wooten MW. Of the atypical PKCs, Par-4 and p62: recent understandings of the biology and pathology of a PB1-dominated complex. Cell Death Differ. 2009; 16:1426–1437. [PubMed: 19713972]

Muller TD, Lee SJ, Jastroch M, Kabra D, Stemmer K, Aichler M, Abplanalp B, Ananthakrishnan G, Bhardwaj N, Collins S, et al. p62 links beta-adrenergic input to mitochondrial function and thermogenesis. The Journal of clinical investigation. 2013; 123:469–478. [PubMed: 23257354]

Nakamura K, Kimple AJ, Siderovski DP, Johnson GL. PB1 domain interaction of p62/sequestosome 1 and MEKK3 regulates NF-kappaB activation. J Biol Chem. 2010; 285:2077–2089. [PubMed: 19903815]

Odegaard JI, Ricardo-Gonzalez RR, Red Eagle A, Vats D, Morel CR, Goforth MH, Subramanian V, Mukundan L, Ferrante AW, Chawla A. Alternative M2 activation of Kupffer cells by PPARdelta ameliorates obesity-induced insulin resistance. Cell Metab. 2008; 7:496–507. [PubMed: 18522831]

Patsouris D, Li PP, Thapar D, Chapman J, Olefsky JM, Neels JG. Ablation of CD11c-positive cells normalizes insulin sensitivity in obese insulin resistant animals. Cell Metab. 2008; 8:301–309. [PubMed: 18840360]

Qatanani M, Lazar MA. Mechanisms of obesity-associated insulin resistance: many choices on the menu. Genes & development. 2007; 21:1443–1455. [PubMed: 17575046]

Rodriguez A, Duran A, Selloum M, Champy MF, Diez-Guerra FJ, Flores JM, Serrano M, Auwerx J, Diaz-Meco MT, Moscat J. Mature-onset obesity and insulin resistance in mice deficient in the signaling adapter p62. Cell Metab. 2006; 3:211–222. [PubMed: 16517408]

Sabio G, Das M, Mora A, Zhang Z, Jun JY, Ko HJ, Barrett T, Kim JK, Davis RJ. A stress signaling pathway in adipose tissue regulates hepatic insulin resistance. Science. 2008; 322:1539–1543. [PubMed: 19056984]

Schenk S, Saberi M, Olefsky JM. Insulin sensitivity: modulation by nutrients and inflammation. J Clin Invest. 2008; 118:2992–3002. [PubMed: 18769626]

Shoelson SE, Lee J, Goldfine AB. Inflammation and insulin resistance. J Clin Invest. 2006; 116:1793–1801. [PubMed: 16823477]

Solinas G, Vilcu C, Neels JG, Bandyopadhyay GK, Luo JL, Naugler W, Grivennikov S, Wynshaw-Boris A, Scadeng M, Olefsky JM, et al. JNK1 in hematopoietically derived cells contributes to diet-induced inflammation and insulin resistance without affecting obesity. Cell Metab. 2007; 6:386–397. [PubMed: 17983584]

Spiegel AM, Nabel EG. NIH research on obesity and type 2 diabetes: providing the scientific evidence base for actions to improve health. Nat Med. 2006; 12:67–69. [PubMed: 16397572]

Takahashi K, Mizuarai S, Araki H, Mashiko S, Ishihara A, Kanatani A, Itadani H, Kotani H. Adiposity elevates plasma MCP-1 levels leading to the increased CD11b-positive monocytes in mice. J Biol Chem. 2003; 278:46654–46660. [PubMed: 13129912]

Tuncman G, Hirosumi J, Solinas G, Chang L, Karin M, Hotamisligil GS. Functional in vivo interactions between JNK1 and JNK2 isoforms in obesity and insulin resistance. Proc Natl Acad Sci U S A. 2006; 103:10741–10746. [PubMed: 16818881]

Ukropcova B, Sereda O, de Jonge L, Bogacka I, Nguyen T, Xie H, Bray GA, Smith SR. Family history of diabetes links impaired substrate switching and reduced mitochondrial content in skeletal muscle. Diabetes. 2007; 56:720–727. [PubMed: 17327442]

Vallerie SN, Furuhashi M, Fucho R, Hotamisligil GS. A predominant role for parenchymal c-Jun amino terminal kinase (JNK) in the regulation of systemic insulin sensitivity. PLoS One. 2008; 3:e3151. [PubMed: 18773087]

Vats D, Mukundan L, Odegaard JI, Zhang L, Smith KL, Morel CR, Wagner RA, Greaves DR, Murray PJ, Chawla A. Oxidative metabolism and PGC-1beta attenuate macrophage-mediated inflammation. Cell Metab. 2006; 4:13–24. [PubMed: 16814729]

Yach D, Stuckler D, Brownell KD. Epidemiologic and economic consequences of the global epidemics of obesity and diabetes. Nat Med. 2006; 12:62–66. [PubMed: 16397571]

Yang JQ, Liu HZ, Diaz-Meco MT, Moscat J. NBR1 is a new PB1 signalling adapter in Th2 differentiation and allergic airway inflammation in vivo. Embo Journal. 2010; 29:3421–3433. [PubMed: 20808283]

Zhang X, Xu A, Chung SK, Cresser JH, Sweeney G, Wong RL, Lin A, Lam KS. Selective inactivation of c-Jun NH2-terminal kinase in adipose tissue protects against diet-induced obesity and improves insulin sensitivity in both liver and skeletal muscle in mice. Diabetes. 2011; 60:486–495. [PubMed: 21270260]

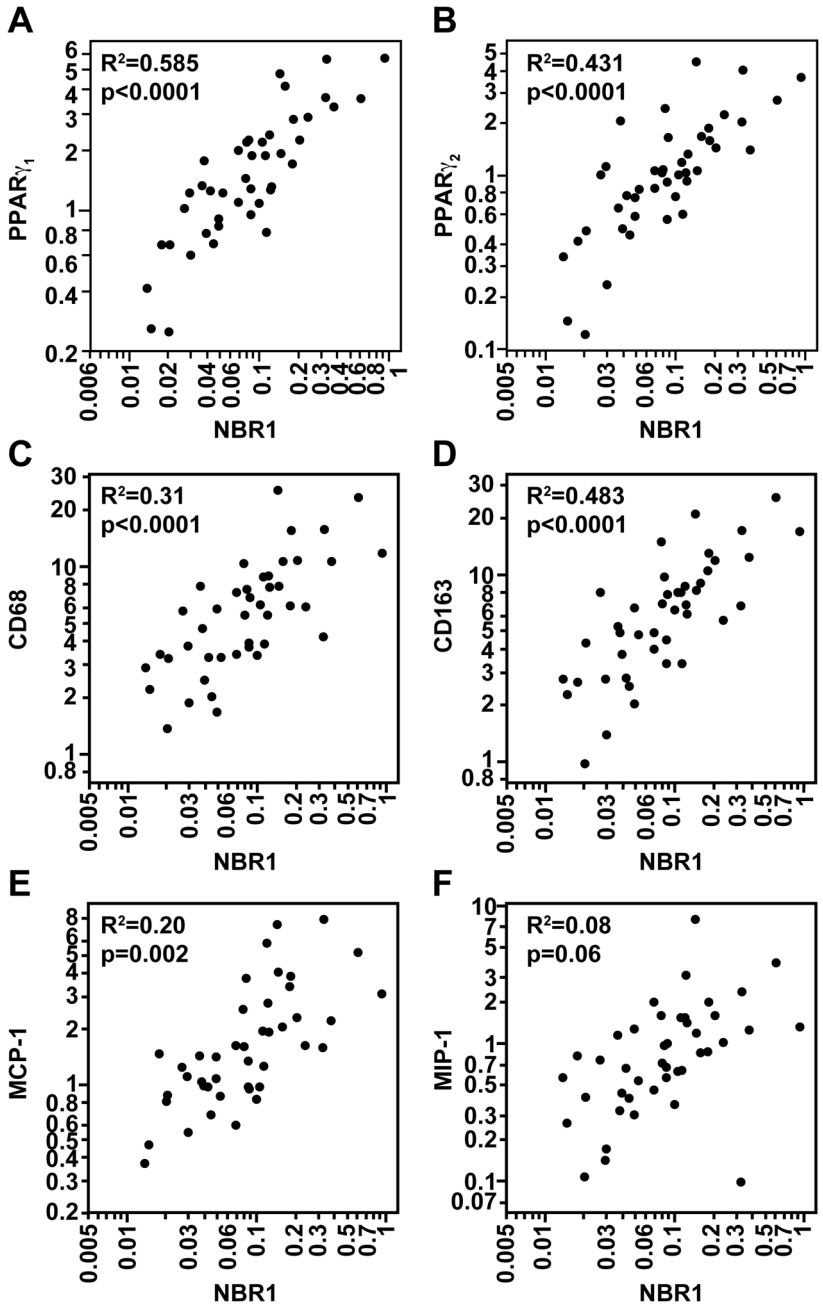

Figure 1. NBR1 transcripts levels correlate with adipose inflammation in obese patients

Positive correlation between transcript levels of NBR1 and PPARγ1 (A), PPARγ2 (B), CD68 (C), CD163 (D), MIP-1 (E) and MCP-1 (F) in obese patients. See also Table S1.

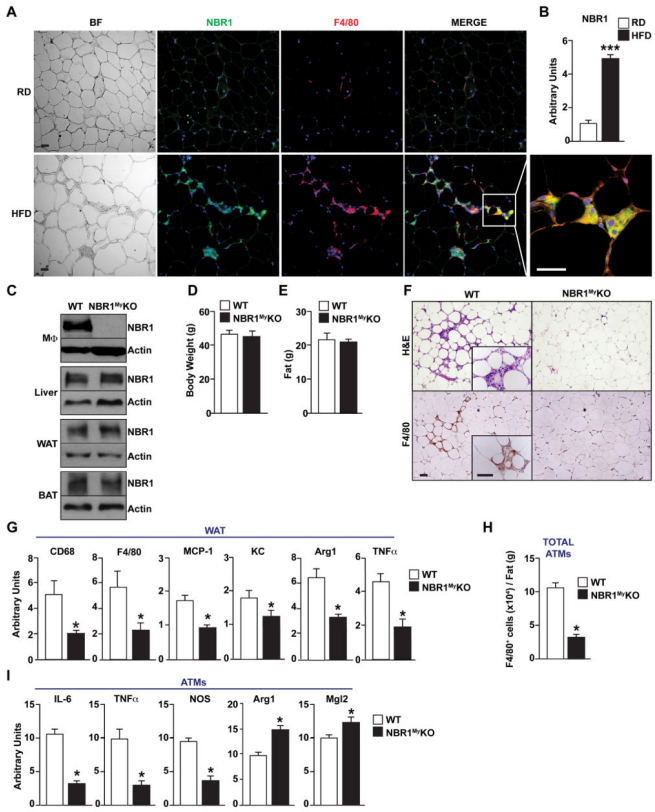

Figure 2. Myeloid-specific deletion of NBR1 reduced ATM and inflammation in HFD-fed mice

A) Immunofluorescence staining for NBR1 (green), F4/80 (red) and DAPI (blue) in epididymal white adipose tissue of RD-fed mice (top) and HFD-fed mice (bottom). Colocalization of NBR1 and F4/80 is shown in yellow in the merged image (n = 5 mice). (B) Quantitative analysis of relative expression of NBR1, as measured by RT-PCR using total RNA isolated from ATMs of RD-fed mice and HFD-fed mice (n = 6–10 mice). (C) NBR1 expression in BMDMs (Mø), liver, epididymal white adipose tissue (WAT) and brown adipose tissue (BAT) of WT and NBR1^{My}KO mice, as assessed by western blotting. Results are representative of three experiments. (D) Body weight and (E) fat mass of WT and NBR1^{My}KO mice fed with HFD (n = 6–8 mice). (F) Morphology and myeloid infiltration of WAT samples from HFD-fed WT and NBR1^{My}KO mice, as assessed by H&E staining and F4/80 immunostaining (n = 6–8 mice). (G) Quantitative analysis of relative expression of markers of inflammation, as measured by RT-PCR assay using total RNA isolated from WAT of WT and NBR1^{My}KO mice (n = 6–8 mice). (H) The stromal vascular fraction (SVF) of epididymal adipose tissue was isolated from WT and NBR1^{My}KO mice fed with HFD (4 weeks) and examined by flow cytometry to detect the total number of F4/80+ adipose tissue macrophages (ATMs) (n = 5 mice). (I) Quantitative analysis of relative expression of markers of inflammation, as measured by RT-PCR using total RNA isolated from ATMs of WT and NBR1^{My}KO mice (n = 5 mice). *p < 0.05, ***p < 0.001. Results are presented as mean ± SEM. Scale bars, 50 μm. See also Figure S1.

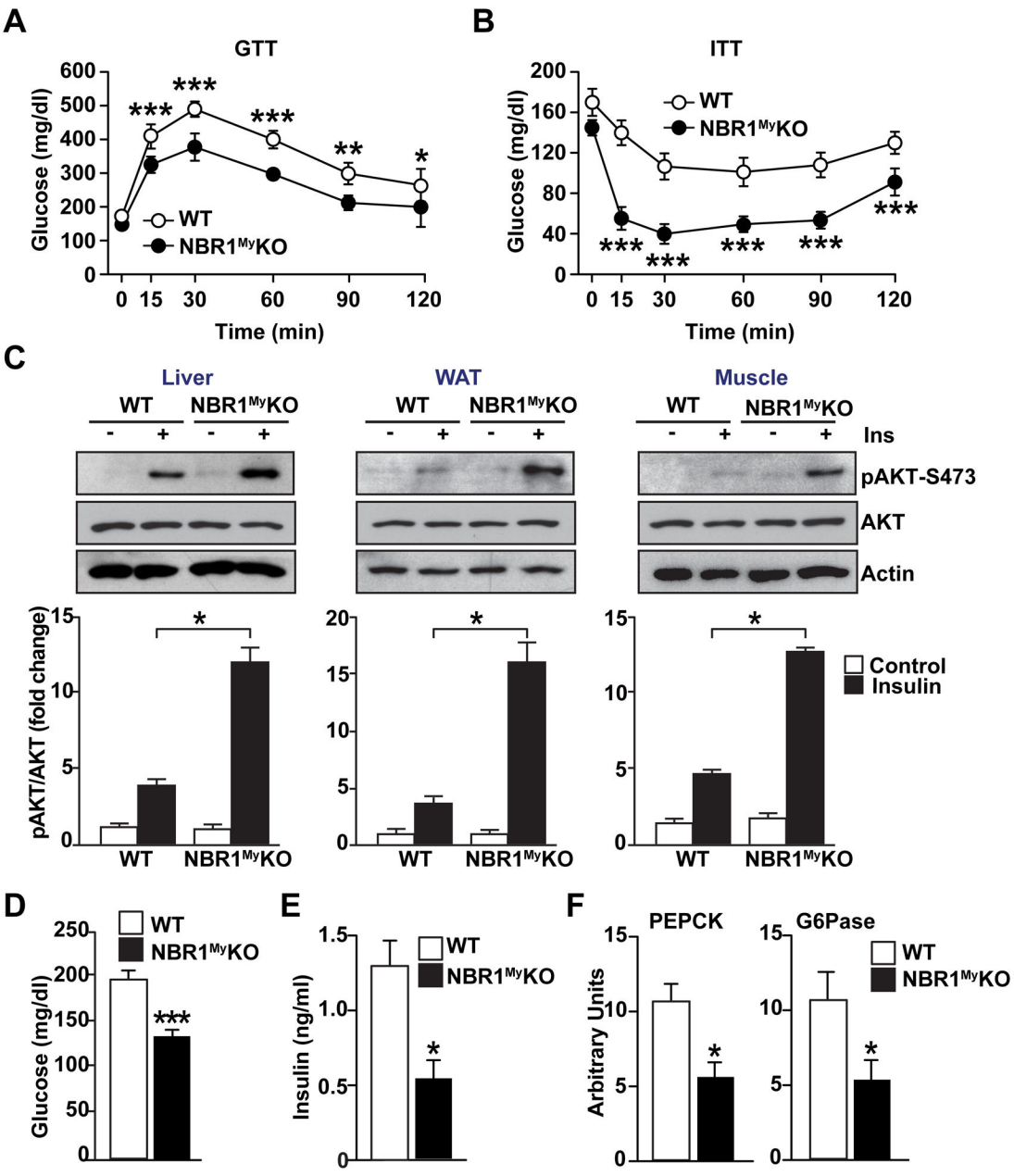

Figure 3. Myeloid-specific deletion of NBR1 improved glucose clearance in HFD-fed mice

(A and B) Glucose tolerance test (GTT) (A) and insulin tolerance test (ITT) (B) in 8-week old WT and NBR1^{My}KO mice fed a HFD for 4 weeks (n = 6–8 mice). (C) WT and NBR1^{My}KO HFD-fed mice were fasted overnight and then treated by i.p. injection with 1 U/kg insulin (15 min). Representative tissue samples were examined by immunoblot analysis by probing with antibodies to phospho-AKT, AKT, and actin. Quantification of phospho-AKT is shown at bottom (n = 5 mice). (D and E) Blood concentration of glucose (D) and insulin (E) in overnight fasted mice HFD-fed WT and NBR1^{My}KO mice (n = 6–8 mice) were measured. (F) Quantitative analysis of relative expression of PEPCK and G6Pase, as measured by RT-PCR using total RNA isolated from livers of HFD-fed WT and

NBR1^{My}KO mice (n = 6–8 mice). *p < 0.05, **p < 0.01, ***p < 0.001. Results are presented as mean ± SEM. See also Figure S2.

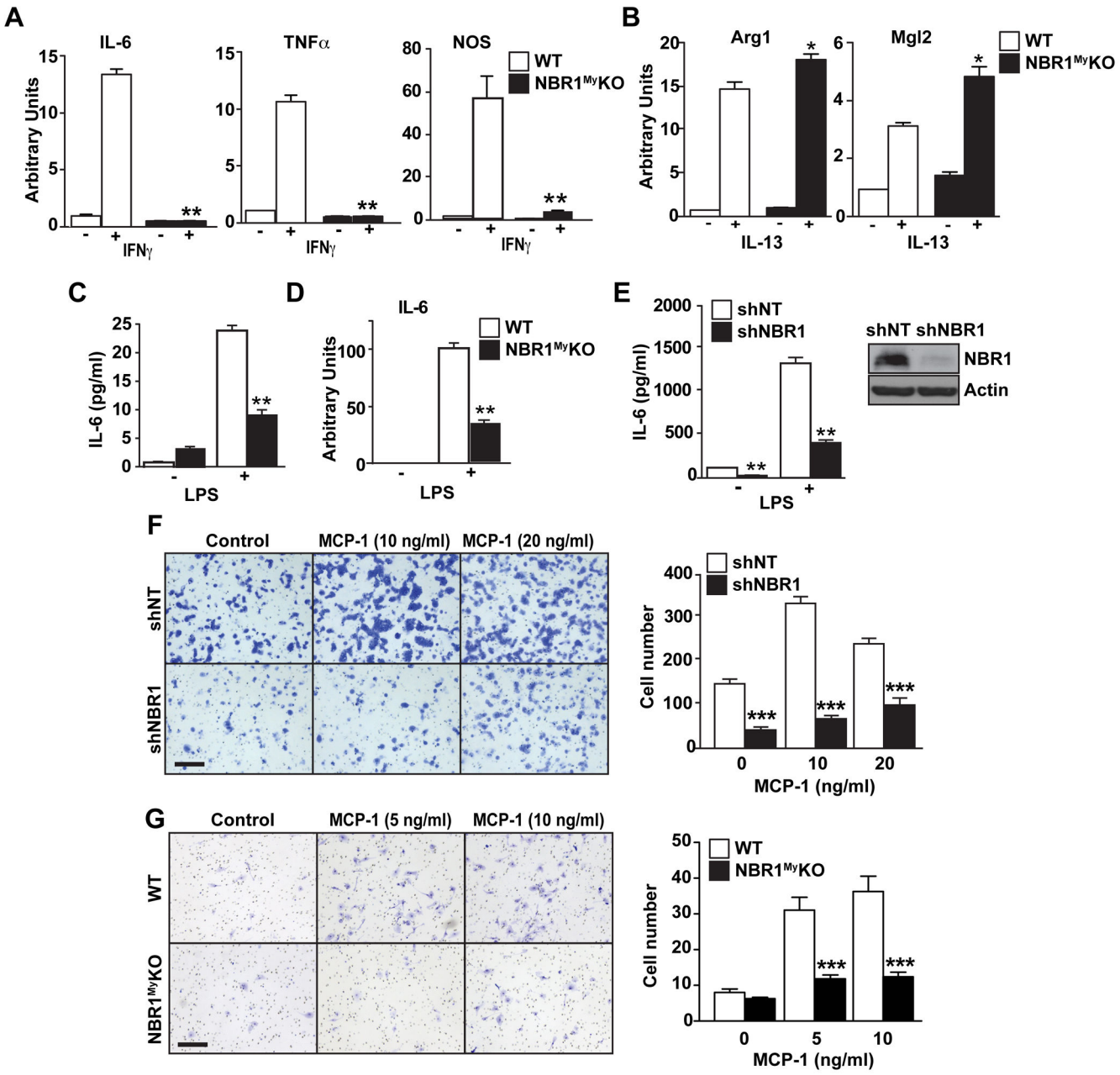

Figure 4. NBR1 deletion in macrophages impaired macrophage polarization toward the pro-inflammatory M1 phenotype

(A and B) Quantitative analysis of relative expression of markers of inflammation. Total RNA was isolated from bone-marrow derived macrophages (BMDMs) of WT and NBR1^{My}KO mice, and incubated with either 100 ng/ml of IFNγ for 8 hr or 10 ng/ml of IL-13 for 72 hr. The relative expression of the indicated markers of M1 (A) or M2 (B) polarization was measured by quantitative RT-PCR assay (n = 6 mice). (C) IL-6 secretion by BMDMs from WT and NBR1^{My}KO mice fed with HFD for 12-weeks, after LPS stimulation (100 ng/ml) for 3 hr (n = 4 mice). (D) Relative expression of mRNA IL-6 by BMDMs from WT and NBR1^{My}KO mice, after LPS stimulation for 8 hr (n = 6 mice). (E) IL-6 secretion by

shNT and shNBR1 Raw cells, after LPS stimulation for 8 hr (F) Migration of shNT and shNBR1 Raw cells after stimulation with the chemoattractant MCP-1 for 20 hr, as determined by a modified Boyden chamber assay. Left panel: representative filters. Right panel: quantitation of data, with total number of cells migrated indicated on y axis. (G) Migration of BMDMs from WT and NBR1^{My}KO mice, treated as in (F). Panels as in (F). Data are representative of three experiments. *$p < 0.05$, **$p < 0.01$, *** $p < 0.001$. Results are presented as mean ± SEM. Scale bars, 100 μm. See also Figure S3.

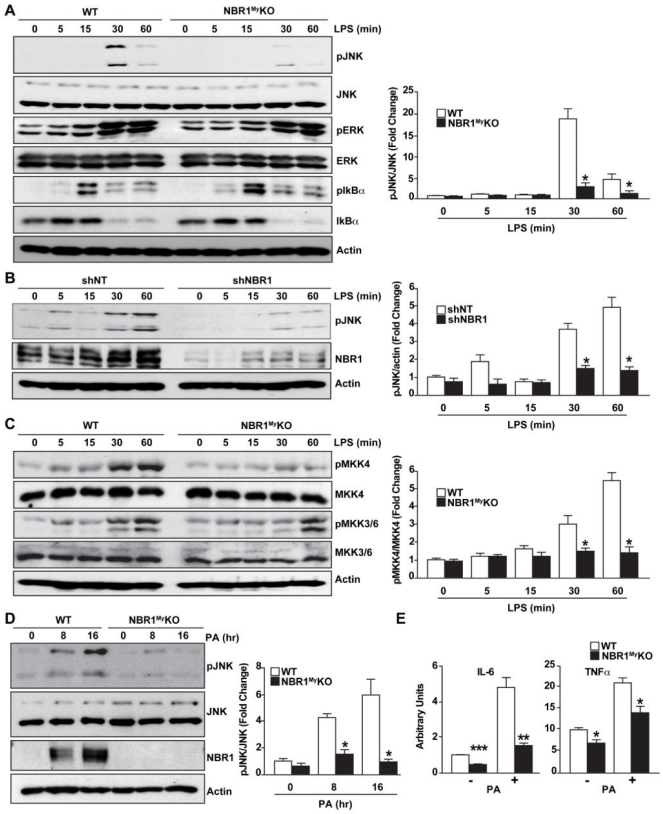

Figure 5. NBR1 deletion in macrophages down-regulated the MEKK2/3-MKK4-JNK pathway

(A–C) Western blot analysis with the indicated antibodies in BMDMs from WT and NBR1^{My}KO mice (A and C) or in shNT- and shNBR1-treated Raw cells (B) stimulated with LPS (100 ng/ml) for the indicated time. Quantification of pJNK (A and B) and pMKK4 (C) fold change activation is shown in the right panels. (D) Western blot analysis with the indicated antibodies in BMDMs from WT and NBR1^{My}KO mice fed a HFD, and stimulated with palmitate (0.8 mM) for the indicated times. Quantification of pJNK fold change activation is shown in the right panel. (E) Quantitative analysis of relative expression of markers of inflammation, as measured by RT-PCR using total RNA isolated from BMDMs of WT and NBR1^{My}KO mice treated as in (D). Data are representative of three experiments. *$p < 0.05$, **$p < 0.01$, ***$p < 0.001$. Results are presented as mean ± SEM.

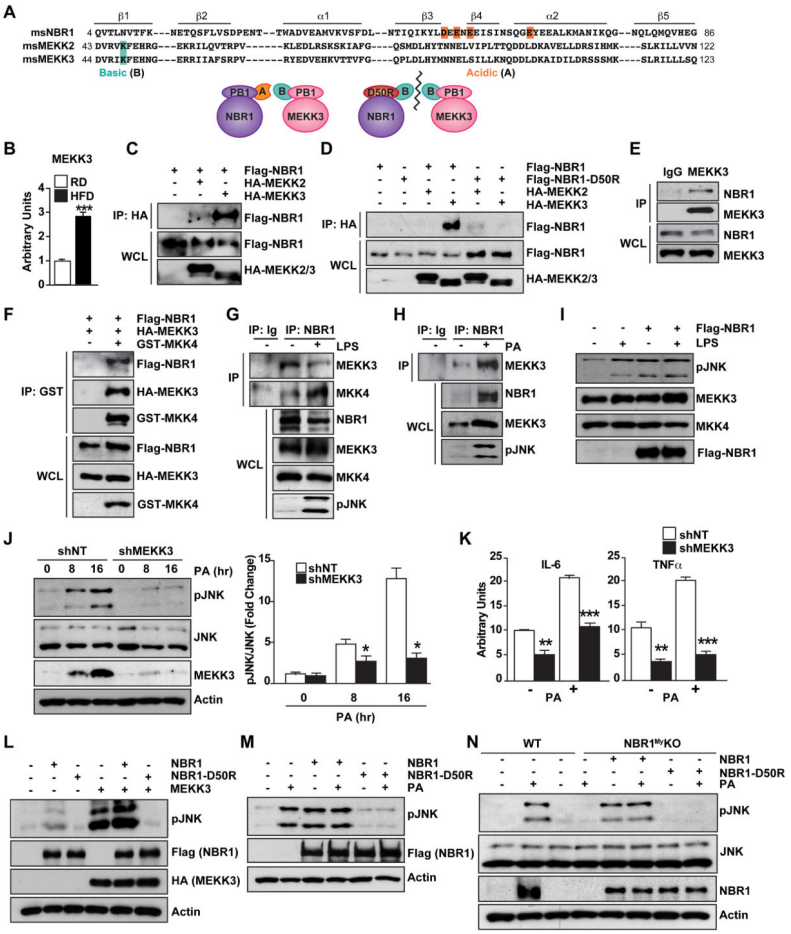

Figure 6. NBR1 is a scaffold for MEKK3 and MKK4

(A) Alignment of amino acid sequence of PB1 domains of mouse NBR1, MEKK2 and MEKK3. The secondary structural elements are shown above the sequences. A conserved basic residue (B) and acidic residues (A) are boxed in green and orange, respectively. The potential interaction between acidic PB1 (PB1-A) of NBR1 and basic PB1 (PB1-B) of MEKK3, and the consequence of the D50R substitution in the PB1 domain of NBR1, are shown in the scheme below the sequences. (B) Quantitative analysis of relative expression of MEKK3, as measured by RT-PCR using total RNA isolated from ATMs of RD-fed mice and HFD-fed mice (n = 6–10 mice). (C and D) Interaction of NBR1 and MEKK3 through the PB1 domain. HEK293T cells were transfected with the indicated plasmids, cell lysates were prepared, and lysates and HA immunoprecipitates were analyzed by western blotting for Flag and HA. (E) Endogenous interaction of NBR1 and MEKK3 was determined in immunoprecipitates from Raw cells by anti-MEKK3 antibody or control IgG. Cell lysates were analyzed by immunoblot. (F) NBR1 is a scaffold for MEKK3 and MKK4. HEK293T cells were transfected with the indicated plasmids, cell lysates were prepared, and lysates and GST immunoprecipitates were analyzed by western blotting. (G) Endogenous interaction of the NBR1-MEKK3-MKK4 complex in LPS-treated cells. HEK-293/hTLR4/MD2/CD14 cells treated with LPS (100 ng/ml) for 30 min were immunoprecipitated with anti-NBR1 antibody or control IgG. Cell lysates and immunoprecipitates were analyzed

by immunoblotting. (H) Endogenous interaction of NBR1 and MEKK3 in palmitate-treated BMDMs. BMDMs were serum starved for 1 hr and stimulated with 0.8 mM palmitate for 16 hr. (I) Overexpression of NBR1 is sufficient to activate JNK. HEK-293/hTLR4/MD2/CD14 cells were transfected with Flag-NBR1 and then stimulated with LPS as in (F). Cell lysates were prepared and immunoblotted for the specified proteins. (J) Western blot analysis of pJNK, JNK and MEKK3 in BMDMs lentivirally infected with shRNA specific for MEKK3, and stimulated with palmitate (0.8 mM) for the indicated times. Quantification of pJNK fold change activation is shown in the right panel. (K) Quantitative analysis of relative expression of markers of inflammation, as measured by RT-PCR using total RNA isolated from BMDMs lentivirally infected with shRNA specific for MEKK3 and treated as in (J). (L and M) Overexpression of NBR1 but not the PB1-mutant NBR1-D50R mediates JNK activation in cotransfection with MEKK3 (L) or after palmitate treatment (M) in 293T cells. (N) Re-expression of NBR1 WT but not of NBR1-D50R reconstituted palmitate-induced JNK activation in NBR1-deficient BMDMs. BMDMs from $NBR1^{My}KO$ mice were reconstituted retrovirally wih FLAG-NBR1 or FLAG-NBR1(D50R) and treated with palmitate as in (J). Cell lysates were prepared and immunoblotted for the specified proteins. Results are representative of two experiments. $^{**}p < 0.01$, $^{***}p < 0.001$. Results are presented as mean ± SEM. See also Figure S4.